Ab initio study of lattice dynamics of group IV semiconductors using pseudohybrid functionals for extended Hubbard interactions

Wooil Yang and Seung-Hoon Jhi *
Department of Physics, Pohang University of Science and Technology, Pohang 37673, Republic of Korea

Sang-Hoon Lee and Young-Woo Son †
Korea Institute for Advanced Study, Seoul 02455, Republic of Korea

(Received 11 June 2021; revised 3 September 2021; accepted 16 September 2021; published 27 September 2021)

We study the lattice dynamics of group IV semiconductors using the fully *ab initio* extended Hubbard functional. The on-site and intersite Hubbard interactions are determined self-consistently with recently developed pseudohybrid functionals and included in force calculations. We analyze the Pulay forces with the choice of atomic orbital projectors and the force contribution of the on-site and intersite Hubbard terms. The phonon dispersions, Grüneisen parameters, and lattice thermal conductivities of diamond, silicon, and germanium, which are the most representative covalent-bonding semiconductors, are calculated and compared with the results using local, semilocal, and hybrid functionals. The extended Hubbard functional produces increased phonon velocities and lifetimes, and thus lattice thermal conductivities compared to local and semilocal functionals, agreeing with experiments very well. Considering that our computational demand is comparable to simple local functionals, this work thus suggests a way to perform high-throughput electronic and structural calculations with higher accuracy.

DOI: 10.1103/PhysRevB.104.104313

I. INTRODUCTION

Density functional theory (DFT) [1,2] has been very successful in the prediction of various physical properties of real materials [3]. Popular practical implementations of DFT treat the electron correlation at the noninteracting one-electron level within the local density approximation (LDA) [2] or the generalized gradient approximation (GGA) [4]. A common, but very serious, problem that may arise from the approximations of electron interaction in LDA and GGA is the errors from improper treatment of the electron self-interaction, known as self-interaction errors (SIEs) [5,6]. Not only for strongly correlated systems but also for conventional covalent-bonding materials, the SIE leads to an incorrect description of the ground systems. Underestimation and overestimation of the lattice constant or the energy band gap are well-known syndromes of these functionals. Such incorrectness in the lattice calculation also leads to errors in elastic properties and phonon spectra.

In order to alleviate the shortcomings associated with the SIE, various modified functionals such as meta-GGA functionals [7–12] and hybrid functionals [13–15] were developed. These approaches still contain empirical parameters to handle the long-range screening and fail to describe strongly correlated localized systems and low-dimensional systems [16]. Another level of approximation to treat many-body electron correlation is to include the dynamic screening in the Coulomb interaction as in the *GW* method [17–19] and dynamical mean-field theory [20]. These methods still require significant computational resources compared to standard DFT, which is impractical for massive calculations of many-atom systems and for extensive high-throughput calculations.

Since SIE is related to the issue of electron localization, a common remedy is to compensate the delocalization error, particularly for d or f electron systems, by introducing the local Coulomb repulsion or the on-site Hubbard U interaction. The DFT $+ U$ method corrects the issue of electron overdelocalization, capturing the essential physics in the Mott insulators and the magnetic ground states [21–24]. However, it fails to describe conventional covalent-bonding semiconductors since the hybridization of the extended orbitals between the pair of atoms is not handled well by the Hubbard U term for the localized sites [25–28]. Campo and Cococcioni introduced the extended Hubbard method into DFT calculations, namely, the DFT $+ U + V$ functional, treating the on-site and intersite Coulomb interactions on equal footing [25]. The DFT $+ U + V$ functional was shown to give the band gap of conventional semiconductors accurately in a similar level of the *GW* method with significantly reduced computational demand [25–28]. Also, the Hubbard U and V terms are essential for describing correctly the properties involved with both strong electron localization and orbital hybridization such as the energetics and structure of transition-metal-oxide molecules [29], the voltage of Li-ion batteries [30], the defect states of oxygen vacancies in perovskites [31], and the x-ray absorption near-edge structures in transition-metal oxides [32].

In typical DFT $+ U$ methods, the on-site Hubbard U is chosen empirically in a reasonable range to produce the standard structural or electronic properties such as the lattice

* jhish@postech.ac.kr
† hand@kias.re.kr

constant and band gap matched to experimental measurements [21–24]. Recently, various methods to compute Hubbard parameters self-consistently were proposed [33–41]. Computation of the Hubbard terms requires the orbital occupation numbers projected into either the nonorthogonalized atomic orbitals (NAOs) or the Löwdin orthonormalized atomic orbitals (LOAOs). While a NAO is simple in code implementation, it tends to overestimate the occupation number and double count the Hubbard correction in the overlap regions [42]. The LOAO requires a demanding procedure for the derivative of the overlap matrix but avoids such errors [28,43]. Among various methods, the pseudohybrid Hubbard density functional proposed by Agapito, Curtarolo, and Buongiorno Nardelli (ACBN0) leads to a direct self-consistent determination of U using Hartree-Fock (HF) formalism with moderate computational cost [41]. In a similar way, the intersite Hubbard V term is implemented in the ACBN0 functional [26,27]. The extended ACBN0 functional determines self-consistently the Hubbard parameters U and V and calculates the band gaps of diverse semiconductors and insulators comparable to those from GW methods with a much lower computational load than GW calculations [26,27]. The self-consistent determination of the Hubbard terms enables accurate computation of lattice dynamics and structural relaxation beyond the one-particle level approximation of LDA or GGA.

In this work, using the recently-developed extended Hubbard functional, we carry out a comparative study of the structural and electronic properties of the group IV semiconductors diamond (C), silicon, and germanium to make point-by-point comparisons with various exchange-correlation functionals. These semiconductors are the most representative covalent-bonding semiconductors, expected to exhibit the apparent correction from the intersite Hubbard term V. We are particularly interested in the lattice dynamics of these semiconductors such as the phonon band structure, the mode Grüneisen parameters, and the thermal conductivity, as they are affected by the Hubbard terms, U and V. The computed static and dynamic lattice properties are in excellent agreement with experiment results, thus demonstrating the effectiveness as well as accuracy of the extended Hubbard functional in studying electronic and structural properties of solids simultaneously.

This paper is organized as follows. We first briefly review our formalism of the pseudohybrid functionals for intersite Hubbard interactions and associated forces in Sec. II. The detailed computational parameters for the calculations of electron energy bands as well as static and dynamic lattice properties are listed in Sec. III. Then, using the method described in Sec. II, we present our computational results for the electronic, structural, and phonon properties of group IV semiconductors in Sec. IV. Finally, we conclude in Sec. V.

II. FORMALISM FOR EXTENDED HUBBARD ENERGY FUNCTIONALS AND FORCES

Here we briefly review the DFT method with U and V interactions [25–28] and a recently developed intersite Hubbard pseudohybrid functional [26,27]. Then, the forces originating from the U and V terms are discussed. We first start by considering the total energy formula with the Hubbard energy functional,

$$E_{\rm tot} = E_{\rm DFT} + E_{\rm Hub}. \tag{1}$$

In Eq. (1), $E_{\rm DFT}$ can be any local or semilocal density functional, and the extended Hubbard functional $E_{\rm Hub}$ is expressed in a rotationally invariant form with $U_{\rm eff} \equiv U - J$ and V with double counting corrections [25],

$$E_{\rm Hub} = \frac{1}{2}\sum_{I}\sum_{i,j,\sigma} U^{I}_{\rm eff}\left(\delta_{ij} - n^{II\sigma}_{ij}\right)n^{II\sigma}_{ji} - \frac{1}{2}\sum_{\{I,J\}}\sum_{i,j,\sigma} V^{IJ} n^{IJ\sigma}_{ij} n^{JI\sigma}_{ji}, \tag{2}$$

where the general occupation matrix is written as

$$n^{IJ\sigma}_{ij} \equiv n^{I,n,l,J,n',l',\sigma}_{ij} = \sum_{m\mathbf{k}} f_{m\mathbf{k}} \langle \psi^{\sigma}_{m\mathbf{k}} | \phi^{I,n,l}_{i} \rangle \langle \phi^{J,n',l'}_{j} | \psi^{\sigma}_{m\mathbf{k}} \rangle \equiv \sum_{m\mathbf{k}} f_{m\mathbf{k}} \langle \psi^{\sigma}_{m\mathbf{k}} | \phi^{I}_{i} \rangle \langle \phi^{J}_{j} | \psi^{\sigma}_{m\mathbf{k}} \rangle. \tag{3}$$

Here $f_{m\mathbf{k}}$ is the Fermi-Dirac function of the Bloch state $|\psi^{\sigma}_{m\mathbf{k}}\rangle$ of the mth band at momentum $\mathbf{k}$. In Eq. (2), $\{I, J\}$ denotes a pair of different atoms within a cutoff distance. The principal (n), azimuthal (l), angular (i), and spin (σ) quantum numbers of the Ith atom are implicitly written in the last line of Eq. (3) and will be used hereafter. The LOAO of ϕ^{I}_{i} [44,45] is used as a projector.

To obtain pseudohybrid functionals for Hubbard interactions, we follow an ansatz by Mosey *et al.* [39,40] and the ACBN0 functional [41], which leads to the "renormalized" occupation number $N^{IJ\sigma}_{\psi_{m\mathbf{k}}}$ and density matrix $P^{IJ\sigma}_{ij}$ for the pair of different atoms I and J:

$$N^{IJ\sigma}_{\psi_{m\mathbf{k}}} = \sum_{\{I\}}\sum_{i} \langle \psi^{\sigma}_{m\mathbf{k}} | \phi^{I}_{i} \rangle \langle \phi^{I}_{i} | \psi^{\sigma}_{m\mathbf{k}} \rangle + \sum_{\{J\}}\sum_{j} \langle \psi^{\sigma}_{m\mathbf{k}} | \phi^{J}_{j} \rangle \langle \phi^{J}_{j} | \psi^{\sigma}_{m\mathbf{k}} \rangle, \tag{4}$$

$$P^{IJ\sigma}_{ij} = \sum_{m\mathbf{k}} f_{n\mathbf{k}} N^{IJ\sigma}_{\psi_{m\mathbf{k}}} \langle \psi^{\sigma}_{m\mathbf{k}} | \phi^{I}_{i} \rangle \langle \phi^{J}_{j} | \psi^{\sigma}_{m\mathbf{k}} \rangle, \tag{5}$$

where $\{I\}$ and $\{J\}$ in Eq. (4) denote all the orbitals with quantum number n and l of a type I atom and a type J atom, respectively. For a pair of the same atoms or for the U calculation, the above expression reduces to $N^{I\sigma}_{\psi_{m\mathbf{k}}} = \sum_{\{I\}}\sum_{i} \langle \psi^{\sigma}_{m\mathbf{k}} | \phi^{I}_{i} \rangle \langle \phi^{I}_{i} | \psi^{\sigma}_{m\mathbf{k}} \rangle$.

The HF energy can be expressed with Eqs. (4) and (5), and the bare Coulomb repulsion between electrons belongs to i and k orbitals of atom I and j and l orbitals of atom J, $(ik|jl) \equiv \int d\mathbf{r}_1 d\mathbf{r}_2 \frac{\phi^{I*}_{i}(\mathbf{r}_1)\phi^{I}_{k}(\mathbf{r}_1)\phi^{J*}_{j}(\mathbf{r}_2)\phi^{J}_{l}(\mathbf{r}_2)}{|\mathbf{r}_1 - \mathbf{r}_2|}$. By inspecting the equivalence between the unrestricted HF formulation and the Dudarev form of extended Hubbard interactions, we can obtain the following functional forms for U^I and J^I [41] and V^{IJ} [26,27] as follows:

$$U^{I} = \sum_{ijkl} \mathcal{U}^{I}_{ijkl}(ij|kl), \quad J^{I} = \sum_{ijkl} \mathcal{J}^{I}_{ijkl}(ik|jl), \tag{6}$$

$$V^{IJ} = \sum_{ij} \mathcal{V}^{IJ}_{ij}(ii|jj). \tag{7}$$

It is immediately noticeable that Hubbard functionals in Eqs. (6) and (7) are weighted Coulomb interactions between electrons belonging to orbitals of the pair atoms. The weight factors can be expressed with Eqs. (3), (4), and (5) such that $\mathcal{U}^I_{ijkl} = \frac{1}{\mathcal{N}^I}\sum_{\sigma,\sigma'} P^{II\sigma}_{ij} P^{II\sigma'}_{kl}$, $\mathcal{J}^I_{ijkl} = \frac{1}{\mathcal{N}^J}\sum_{\sigma} P^{II\sigma}_{ij} P^{II\sigma}_{kl}$, and $\mathcal{V}^{IJ}_{ij} = \frac{1}{2\mathcal{N}^{IJ}}\sum_{\sigma,\sigma'}[P^{II\sigma}_{ii} P^{JJ\sigma'}_{jj} - \delta_{\sigma\sigma'} P^{IJ\sigma}_{ij} P^{JI\sigma'}_{ji}]$, where the normalization factors are $\mathcal{N}^I = \sum_{i\neq j}\sum_{\sigma} n^{II\sigma}_{ii} n^{II\sigma}_{jj} + \sum_{ij}\sum_{\sigma} n^{II\sigma}_{ii} n^{II-\sigma}_{jj}$, $\mathcal{N}^J = \sum_{i\neq j}\sum_{\sigma} n^{II\sigma}_{ii} n^{II\sigma}_{jj}$, and $\mathcal{N}^{IJ} = \sum_{\sigma,\sigma'}\sum_{ij}[n^{II\sigma}_{ii} n^{JJ\sigma'}_{jj} - \delta_{\sigma\sigma'} n^{IJ\sigma}_{ij} n^{JI\sigma'}_{ji}]$. We note that the weight factors could be regarded as the position-dependent mixing parameters of HF interactions reflecting local changes of Coulomb interactions as well as the nonlocal variation for intersite screenings.

Forces from extended Hubbard interactions on the Kth atom can be obtained using the derivative of $E_{\rm Hub}$ in Eq. (2) with respect to its displacement of $\mathbf{R}_K$ [27,43]. Using the chain rule,

$$\frac{\partial E_{\rm Hub}}{\partial \mathbf{R}_K} = \sum_I \sum_{i,j,\sigma} \frac{\partial E_{\rm Hub}}{\partial n^{II\sigma}_{ij}} \frac{\partial n^{II\sigma}_{ij}}{\partial \mathbf{R}_K} + \sum_I \frac{\partial E_{\rm Hub}}{\partial U^I_{\rm eff}} \frac{\partial U^I_{\rm eff}}{\partial \mathbf{R}_K} + \sum_{\{I,J\}} \frac{\partial E_{\rm Hub}}{\partial V^{IJ}} \frac{\partial V^{IJ}}{\partial \mathbf{R}_K}. \tag{8}$$

After some algebra, each contribution to the total Hubbard force $\mathbf{F}_{\rm Hub} \equiv \partial E_{\rm Hub}/\partial \mathbf{R}_K = \mathbf{F}^N + \mathbf{F}^U + \mathbf{F}^V$ can be written as

$$\mathbf{F}^N \equiv \sum_I \sum_{i,j,\sigma} U^I_{\rm eff}\left(\frac{\delta_{ij}}{2} - n^{II\sigma}_{ij}\right)\frac{\partial n^{II\sigma}_{ji}}{\partial \mathbf{R}_K} - \sum_{\{I,J\}}\sum_{i,j,\sigma} V^{IJ} n^{IJ\sigma}_{ij} \frac{\partial n^{JI\sigma}_{ji}}{\partial \mathbf{R}_K}, \tag{9}$$

$$\mathbf{F}^U \equiv \frac{1}{2}\sum_I \sum_{i,j,\sigma} \frac{\partial U^I_{\rm eff}}{\partial \mathbf{R}_K}\left(\delta_{ij} - n^{II\sigma}_{ij}\right) n^{II\sigma}_{ji}, \tag{10}$$

$$\mathbf{F}^V \equiv -\frac{1}{2}\sum_{\{I,J\}}\sum_{i,j,\sigma} \frac{\partial V^{IJ}}{\partial \mathbf{R}_K} n^{IJ\sigma}_{ij} n^{JI\sigma}_{ji}. \tag{11}$$

In calculating $\partial n^{II\sigma}_{ji}/\partial \mathbf{R}_K$ in Eq. (9), the main contribution comes from a derivative of the LOAO, $\partial \phi^{I,n,l}_i/\partial \mathbf{R}_K$, so that $\mathbf{F}^N$ can be regarded as the Pulay force [43]. Unlike NAO projectors, $\partial n^{II\sigma}_{ji}/\partial \mathbf{R}_K$ in Eq. (9) is not zero in the case of $I \neq J \neq K$ [43], and neither are $\partial U^I_{\rm eff}/\partial \mathbf{R}_K$ in Eq. (10) and $\partial V^{IJ}/\partial \mathbf{R}_K$ in Eq. (11). The difficulty in evaluating the derivative of the LOAO [27,43] was overcome by Timrov *et al.* [43] recently, so direct evaluation of $\mathbf{F}^N$ is now feasible.

Typically, $\mathbf{F}^U$ and $\mathbf{F}^V$ are quite small and have been neglected so far [27,30,43], although for some metal-oxide molecules $\mathbf{F}^U$ is not negligible [46]. Since we compute the on-site and intersite Hubbard interactions self-consistently, we can check the order of magnitude of forces from Eqs. (10) and (11) directly. For the semiconducting materials here, the forces from the variation of directional bonding are the most significant, so we can simplify Eqs. (10) and (11) as

$$\mathbf{F}^U \simeq \frac{1}{2}\sum_{i,j,\sigma} \frac{\partial U^K_{\rm eff}}{\partial \mathbf{R}_K}\left(\delta_{ij} - n^{KK\sigma}_{ij}\right) n^{KK\sigma}_{ji}, \tag{12}$$

$$\mathbf{F}^V \simeq -\frac{1}{2}\sum_{\{J\}}\sum_{i,j,\sigma} \frac{\partial V^{KJ}}{\partial \mathbf{R}_K} n^{KJ\sigma}_{ij} n^{JK\sigma}_{ji}, \tag{13}$$

where $\{J\}$ in Eq. (13) indicates the sum of contributions of the Jth atom whose distance with respect to the Kth atom is within a given cutoff distance.

III. COMPUTATIONAL DETAILS

All DFT calculations were performed with QUANTUM ESPRESSO [47] and norm-conserving pseudopotentials (NC-PPs) from the Pseudo Dojo library [48]. In the case of LDA, Perdew-Burke-Ernzerhof revised for solids (PBEsol), and the extend Hubbard functionals, the Brillouin zone sampling was done on a k-point grid with a $15 \times 15 \times 15$ mesh to calculate the equilibrium lattice parameter and bulk modulus and on a k-point grid with a $21 \times 21 \times 21$ mesh for electronic structure calculations. For Heyd-Scuseria-Ernzerhof (HSE) hybrid functional calculations, we used $7 \times 7 \times 7$ grids for both calculations. The volume dependence of the static lattice energy was fitted to Vinet's equation of state [49]. The band structure in HSE calculations was obtained via Wannier interpolation [50] using WANNIER90 [51]. Once the Kohn-Sham states are obtained at each self-consistent loop in QUANTUM ESPRESSO, the Hubbard U and V parameters are readily calculated from Eqs. (6) and (7) and used in the next self-consistent loop as implemented in the extended ACBN0 functional [26]. The on-site U for s orbitals was set to be zero. The cutoff energy was set to be 100 Ry, and the self-consistency threshold for the total energy and Hubbard interactions was 10^{-8} Ry. The cutoff distance for intersite V was set to include the nearest neighbors, which is enough for the convergence of total energy of group IV semiconductors [26].

Since the self-consistent U and V terms are expressed in terms of the localized-orbital projectors, the site-dependent Pulay forces naturally arise. The choice of the atomic orbital projectors is thus a critical step in practical implementation for calculating U and V terms and the forces. Here we employ the method implemented by Timrov *et al.* [43] that calculates the Pulay force and stress using orthogonalized atomic wave functions as projectors. To address lattice dynamics, the Pulay force and the derivatives of the Hubbard U and V terms should be calculated correctly in addition to the standard DFT forces. We analyzed the contribution of each force and the errors from inaccurate estimate of the occupation number in the interstitial regions. We found that the Hubbard forces from the derivative of U and V are very small and thus can be neglected in the force calculations, as discussed in Appendix A.

The harmonic and cubic anharmonic interatomic force constants (IFCs) of phonons were calculated using the frozen-phonon method [52,53] in a supercell of 64 atoms with a k-point grid with a $5 \times 5 \times 5$ and $3 \times 3 \times 3$ mesh, respectively. For HSE calculations, the k-point grid was reduced to $2 \times 2 \times 2$ due to the heavy computational cost (Appendix C). We chose atomic displacements of 0.01 Å for the harmonic IFCs and 0.03 Å (C) and 0.04 Å (Si, Ge) for the cubic IFCs. The thermal conductivity was calculated using the phonon Boltzmann transport equation (BTE) [53–62]. We employed the relaxation time approximation (RTA) [63] to calculate the phonon lifetime for Si and Ge since the umklapp scattering is relatively strong around room temperature [54,64]. However, for C, the normal process dominates the umklapp process

TABLE I. Calculated U and V for s and p orbitals (in eV). U_p is the on-site Hubbard term for the p orbital, and V_{ss}, V_{sp}, and V_{pp} are the intersite Hubbard terms between s-s, s-p, and p-p orbitals of the nearest atoms, respectively.

	U_p	V_{ss}	V_{sp}	V_{pp}
C	5.91	0.82	1.09	2.92
Si	3.51	0.88	0.72	1.86
Ge	3.33	1.03	0.70	1.76

[55,59,60], and its lattice thermal conductivity within RTA is severely underestimated compared with the full converged solution [55]. The lattice thermal conductivity of C was calculated with the direct solution of the linearized phonon BTE [65,66].

IV. COMPUTATIONAL RESULTS

Calculated U and V values for C, Si, and Ge at the experimental lattice constants are presented in Table I. U and V of Si are almost the same as in a previous study [26]. Our calculated values are in good agreement with the ones in the literature. We note that the intersite V term is about 25%–50% of the on-site U term in these covalent semiconductors and thus should be correctly determined for accurate description of physical properties. Before proceeding to the lattice dynamics, we calculated the lattice constants, the bulk modulus, and the electronic band structures with various exchange correlations for point-by-point comparison.

A. Structural parameters

Calculated lattice constants and bulk moduli of group IV elements calculated with various functionals are presented in Tables II and III together with experiment values for comparison. Each functional using NC-PPs gives a result similar to the previous DFT calculations using various pseudopotentials [75–79]; LDA underestimates the lattice constants and thus gives a hardened bulk modulus compared with experiment, while PBE overestimates the lattice constants and consequently gives soft bulk moduli. PBEsol and HSE give improved lattice constants and bulk moduli. Compared to these one-electron-based functionals, DFT with the on-site U and intersite Hubbard V terms gives very accurate lattice constants and bulk moduli within 0.2% and 3% of errors overall compared with measurement. This finding is consistent with a previous report [25]. The extended Hubbard functional describes the covalent bonding character properly not only at the static level but also at the dynamic level, as we discuss below.

TABLE II. Optimized theoretical lattice constants (in Å) calculated with LDA, PBE, PBEsol, HSE, and the extended Hubbard functional ($U + V$). Experimental values are measured at ambient conditions.

	LDA	PBE	PBEsol	HSE	$U + V$	Expt.
C	3.537	3.572	3.558	3.558	3.562	3.567[a]
Si	5.394	5.469	5.431	5.434	5.434	5.431[b]
Ge	5.621	5.764	5.676	5.629	5.662	5.658[c]

[a]Reference [67].
[b]Reference [68].
[c]Reference [69].

TABLE III. Optimized bulk modulus (in GPa) calculated with LDA, PBE, PBEsol, HSE, and the extended Hubbard functional ($U + V$). Experimental values are measured at ambient conditions.

	LDA	PBE	PBEsol	HSE	$U + V$	Expt.
C	465	432	449	464	450	442[a]
Si	96	88	93	99	95	96–99.4[b]
Ge	72	59	67	74	72	75–75.8[c]

[a]Reference [70].
[b]References [71,72].
[c]References [73,74].

B. Electronic band structures

Our calculated electronic band structures for group IV semiconductors are shown in Fig. 1, and the fundamental energy gaps are summarized in Table IV. The range of our calculated band gaps is comparable with experimental data. The on-site Hubbard U does not improve the energy band gaps of semiconductors [25–27]. It is clear that the intersite Hubbard V term increases the band gap of group IV semiconductors, consistent with previous reports [25–27]. For a proper description of the covalent sp^3 hybridization, the intersite interaction should be included. We note that, for Ge, the band gap is calculated without considering the spin-orbit interaction and the minimum gap is direct at Γ.

The highest valence band in the extended Hubbard functional is shifted slightly lower than those of PBEsol, HSE, and the GW approximation [86]. Overall, the valence bands in the extended Hubbard functional exhibit dispersions similar to those in PBEsol and also in GW calculations (Si and Ge) [86]. We observe wide bandwidth in the valence bands and a rigid shift of about 1 eV of the lowest-lying valence band in HSE results due to the strong coupling between the valence p band and the conduction s band [75,87]. On the other hand, the on-site U of the s orbital is zero, and no meaningful shift of the lowest-lying s band from the PBEsol band is observed in the extended Hubbard functional.

The conduction bands in the extended Hubbard functional show a rigid shift to higher energies compared to those in PBEsol. The lowest conduction band in the extended Hubbard functional is similar to that in HSE but slightly lower in energy than that in the GW method [86]. The extend Hubbard functionals may be regarded as a static approximation to the GW approximation [22,26,27] expected to produce accuracy comparable to the GW method.

C. Phonon band structures and Grüneisen parameters

We studied the lattice dynamics of group IV semiconductors to demonstrate how the intersite Hubbard V term describes the covalent bonding properly. All calculations were performed at the experimental lattice constant of C

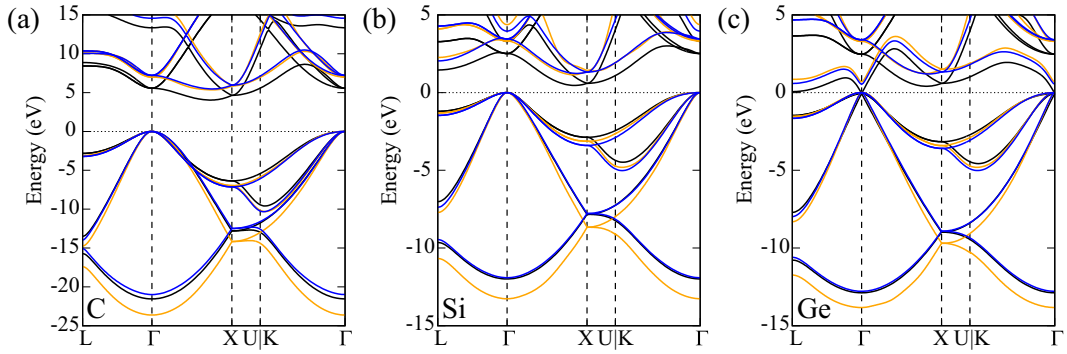

FIG. 1. Calculated electronic band structures of C, Si, and Ge along the symmetry lines in the Brillouin zone using PBEsol (black), HSE (orange), and the extend Hubbard functional (blue). The top of the valence band is set to 0 eV.

(3.5670 Å) and Si (5.4310 Å) at room temperature [67,68] and of Ge (5.6524 Å) at 80 K [69]. Normally, the optimized lattice constant by a specific functional is used for the lattice dynamics and electronics structures. However, apparently good agreement with experiment sometimes comes from the cancellation, for instance, in the LDA case, of the underestimation of the lattice constants and the vibrational frequencies to some extent [75]. Here we chose to confirm the correction by the intersite Hubbard V term in the extended Hubbard functional compared to LDA, PBE, PBEsol, and HSE under the same conditions. Using the finite-difference method, we calculated the IFCs up to second order for the phonon band structures and the third order for the Grüneisen parameters. In the extended Hubbard functional, the Pulay forces arise inevitably from the local atomic orbital basis, and we employed the recently developed method of Timrov *et al.* [43] to handle the orthogonal atomic orbitals. In the extended Hubbard functional, implementation of the self-consistent calculation of U and V is naturally done with atom-centered orthogonal orbitals, but the force calculation can be complicated (see Appendix B for the analysis of the latent errors from inaccurate estimation of the occupation number in the overlap regions of the Pulay forces).

Figures 2(a)–2(c) show calculated phonon band structures at the experimental lattice constants. Calculated phonon bands with the extended Hubbard functional are in very good agreement with experiment compared to the bands from other functionals. Overall, the local and semilocal functionals underestimate the phonon frequencies, and nonlocal HSE overestimates them. As such, the phonon bands of the extended Hubbard functional are located between those of LDA/PBEsol and HSE. A slight overestimation of phonon frequencies by HSE is due to the enhancement of interatomic interaction between neighboring atoms by the inclusion of nonlocal exact exchange compared to PBEsol [75].

The phonon frequencies at high-symmetry points are shown in Table V for a detailed comparison. We note that our calculated phonon frequencies for diamond using the extended Hubbard functional of 39.9, 36.3, and 37.9 THz at the Γ, X, and L point, respectively, are comparable to the harmonic phonon frequencies obtained with the variational quantum Monte Carlo method of 40.7, 36.5, and 38.0 THz [95].

We next calculated the mode Grüneisen parameters of C, Si, and Ge from cubic IFCs to see how well the extended Hubbard functional describes the response of the interatomic forces in covalent bonding systems to volume changes. Calculated mode Grüneisen parameters together with available experimental data are plotted in Figs. 3(a)–3(c). All the functionals here give negative Grüneisen parameters in the transverse acoustic modes for Si and Ge, which explains their negative thermal expansion [96,97]. We observe quite a difference between the functionals in the transverse acoustic branches of Si and Ge. Apparently, the variation in the

TABLE IV. Calculated and measured (Expt.) band gaps (in eV). E_g^d is the direct band gap at the Γ point; E_g^i is the indirect band gap. For Ge, the spin-orbit interaction is not considered in the calculation, and the minimum gap is direct at Γ.

	PBEsol		HSE		$U+V$		Expt.	
	E_g^i	E_g^d	E_g^i	E_g^d	E_g^i	E_g^d	E_g^i	E_g^d
C	4.04	5.56	5.36	7.00	5.47	7.22	5.48[a]	7.3[b]
Si	0.46	2.51	1.15	3.32	1.23	3.46	1.12[c]	3.40[d]
Ge	0.13	0.01	0.85	0.70	0.59	0.54	0.66[e]	0.80[f]

[a]Reference [80].
[b]Reference [81].
[c]Reference [82].
[d]Reference [83].
[e]Reference [84].
[f]Reference [85].

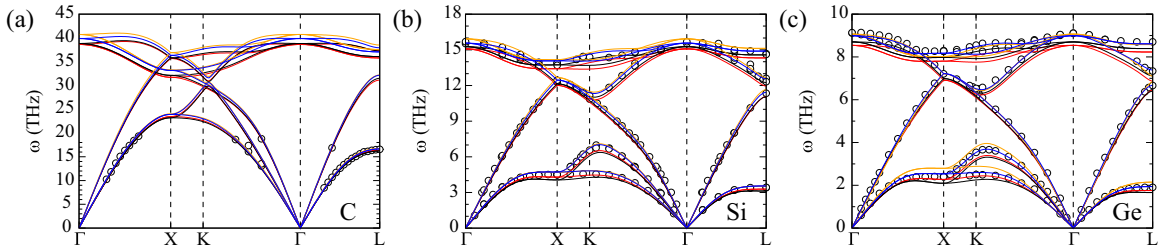

FIG. 2. Calculated phonon band structures of (a) C, (b) Si, and (c) Ge. The phonon bands were obtained at the experimental lattice constant with the exchange-correlation functional of LDA (red), PBEsol (black), HSE (orange), and the extended Hubbard functional (blue). Open circles denote the experimental values for C [88–90], Si [91–93], and Ge [94].

Grüneisen parameters between the functionals reflects the difference in the phonon dispersions of the low-frequency transverse acoustic modes. Compared to experiment, the extended Hubbard functional reproduces very accurately the small Grüneisen parameters of Si, which is related to its weak anharmonicity. While all functionals give results in agreement with the experimental values at the Γ, X, W, and L points in the transverse acoustic modes, the extended Hubbard functional produces results more accurate than those of the LDA and PBEsol functionals. As the transverse acoustic modes are characterized by the noncentral covalent bonding [96], inclusion of the V term in Hubbard functionals captures such features of the covalent bonding appropriately.

We also calculated the mode Grüneisen parameters directly from the volume derivative of the phonon frequencies as a consistency check (right column of Fig. 3). The Grüneisen parameters obtained from cubic IFCs and the direct derivative are similar overall, while the direct volume derivative seems to provide better results than cubic IFCs, especially for Ge, as it captures properly the long-range nature of force constants. We observe wider variation between the two methods for Ge in the extended Hubbard functional than in other mean-field type functionals. This finding again reflects the fact that the extended Hubbard functional describes correctly the relatively delocalized covalent bonding of Ge compared to C and Si. Our calculated Grüneisen parameters show that the extended Hubbard functional gives weaker phonon anharmonicity than LDA or PBEsol. It is known that LDA and GGA, the mean-field approximation to the self-energy interactions, fail to describe properly the localization and delocalization of electrons [105]. These functionals depict the orbital occupation as a continuous function of the bond length and likely to overcount the orbital hybridization as the interatomic distance is changed. The apparent stronger anharmonicity of LDA and PBEsol than in the extended Hubbard functional in our calculations is attributed to this shortcoming.

D. Lattice thermal conductivity and phonon lifetime

Finally, we investigated the thermal transport using the extended Hubbard functional to compare it with other functionals. Figure 4 shows the calculated lattice thermal conductivity and phonon lifetime together with experimental results. Because of weak umklapp scattering relative to the normal scattering in C, the thermal conductivity obtained from BTE within RTA is severely underestimated [55,59,60], and

TABLE V. Our calculated phonon frequencies at high-symmetry points obtained at the experimental lattice constants. Measurements are from Refs. [88,91,92,94].

		$\Gamma_{LO/TO}$	X_{TA}	$X_{LA/LO}$	X_{TO}	L_{TA}	L_{LA}	L_{LO}	L_{TO}
C	LDA	38.6	23.4	35.7	31.7	16.4	31.1	37.3	35.8
	PBEsol	38.8	23.2	35.8	32.1	16.2	31.5	37.3	36.1
	HSE	40.7	24.0	36.9	33.2	16.7	32.2	38.5	37.6
	$U+V$	39.9	23.9	36.3	33.1	16.5	32.1	37.9	37.1
	Expt.[a]	40.3	24.2	36.1	32.6	16.4	31.0	37.2	36.3
Si	LDA	15.1	4.3	12.0	13.4	3.3	11.1	12.0	14.3
	PBEsol	15.3	4.1	12.1	13.7	3.1	11.1	12.3	14.6
	HSE	15.9	4.7	12.7	14.2	3.5	11.7	12.7	15.1
	$U+V$	15.6	4.7	12.5	14.1	3.5	11.4	12.6	14.9
	Expt.[b]	15.5	4.5	12.3	13.9	3.4	11.4	12.6	14.7
Ge	LDA	8.54	2.28	6.91	7.80	1.75	6.44	6.87	8.23
	PBEsol	8.70	2.10	6.99	7.98	1.66	6.40	7.11	8.39
	HSE	9.06	2.79	7.21	8.02	2.15	6.84	7.09	8.58
	$U+V$	8.99	2.53	7.22	8.17	1.94	6.67	7.39	8.61
	Expt.[c]	9.11	2.40	7.22	8.27	1.89	6.66	7.34	8.69

[a]Reference [88].
[b]References [91,92].
[c]Reference [94].

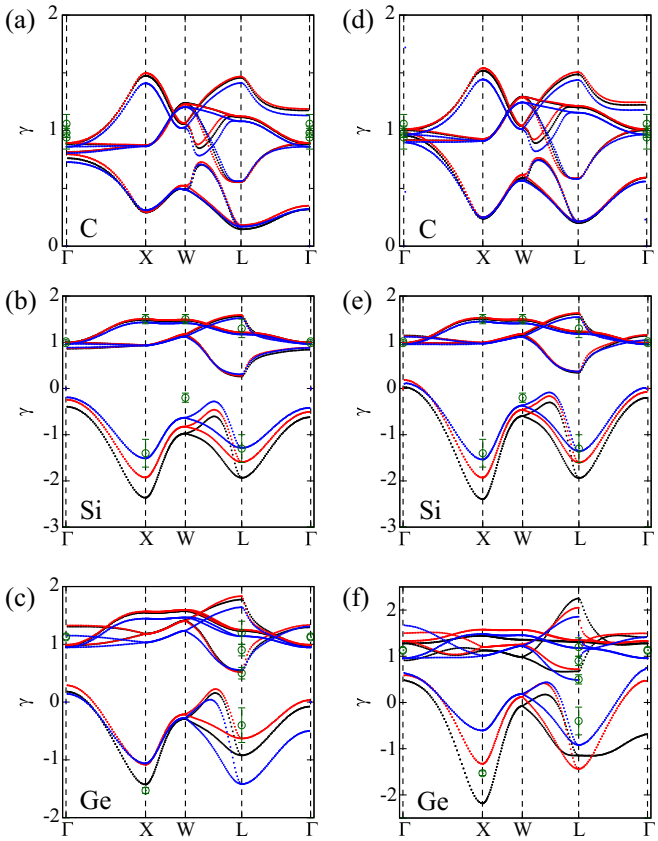

FIG. 3. The mode Grüneisen parameters γ obtained from cubic IFCs (left column) and the volume derivative of the phonon frequencies (right column) with LDA (red), PBEsol (black), and the extended Hubbard functional (blue) for C, Si, and Ge, from top to bottom. Green open circles denote the measured values of C [98–100], Si [101,102], and Ge [101,103,104].

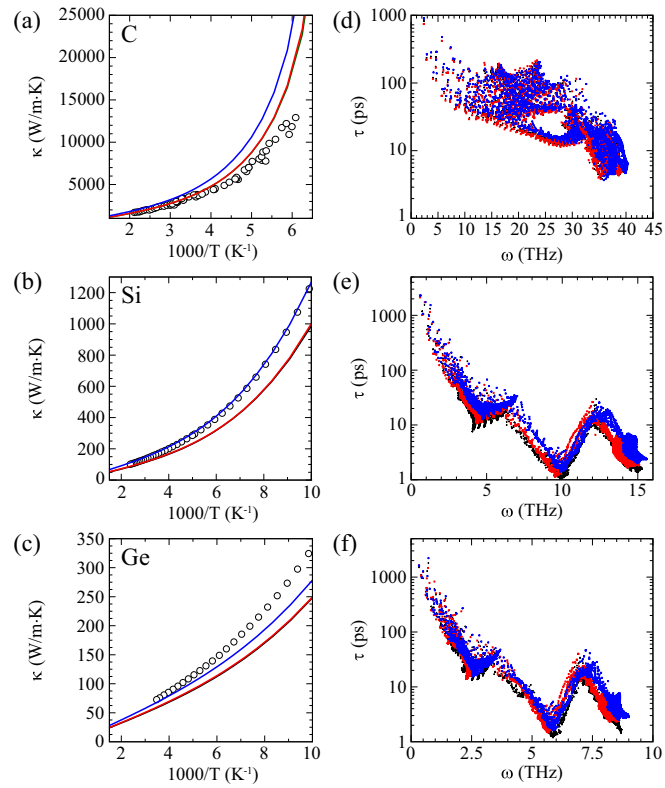

FIG. 4. Calculated lattice thermal conductivity κ (left column) as a function of temperature T and phonon lifetime τ (right column) as a function of the frequency ω of diamond, Si, and Ge, from top to bottom. PBEsol, black; LDA, red; the extended Hubbard functional, blue. PBEsol and the LDA give almost identical results. Experimental values of lattice thermal conductivity (C [106,107], Si [108], and Ge [109,110]) are plotted with open circles.

instead, we used the direct solution of the linearized phonon BTE [65,66].

Our LDA and PBEsol calculations are almost identical and produce similar or slightly smaller values for C at low temperature but underestimate values for Si and Ge compared to experiment [106–110]. It is known that the thermal conductivity of diamond is very sensitive to the isotopic composition [55], and measured values should be smaller than theoretical calculations. The reason for the difference is our choice of the experimental lattice constants for phonon calculations to analyze the functional dependence on the same footing. The phonon group velocity and thus the thermal conductivity are very sensitive to the lattice constants. It was shown that the increase in the lattice constant by 1% in Si results in a decrease of the lattice thermal conductivity by 4% [111]. The apparent agreement of the LDA calculation with experiment in previous studies [55,112,113] is likely attributed to error cancellation of underestimated lattice constants. Also, while calculated lattice thermal conductivity within RTA is close

TABLE VI. The Hubbard forces (in units of Ry/Bohr radius) for the displacement along the [111] direction. R_K is the C-C displacement (in units of the Bohr radius); $F^U + F^V$ is the derivative of U and V. The Pulay forces are calculated with orthogonal (LOAO) and nonorthogonal atomic (NAO) bases with elongated (+) and contractive (−) displacements. Total forces are also shown for comparison with the Hubbard forces.

		LOAO				NAO	
		F^N		$F_{\rm tot}$		F^N	
R_K	$F^U + F^V$	+	−	+	−	+	−
0.025	−0.000010	−0.000076	0.000067	−0.019694	0.020664	−0.000284	0.000266
0.050	0.000014	−0.000167	0.000119	−0.038431	0.042291	−0.000590	0.000506
0.075	0.000153	−0.000271	0.000157	−0.056189	0.064879	−0.000913	0.000713
0.100	0.000253	−0.000387	0.000176	−0.072972	0.088428	−0.001250	0.000883

TABLE VII. The same as Table VI, but for total and Hubbard forces for Si-Si displacement.

		LOAO				NAO	
		F^N		F_{tot}		F^N	
R_K	$F^U + F^V$	+	−	+	−	+	−
0.025	0.000032	−0.000005	0.000003	−0.007029	0.007314	−0.000106	0.000098
0.050	0.000044	−0.000014	0.000002	−0.013778	0.014914	−0.000220	0.000186
0.075	0.000064	−0.000026	−0.000004	−0.020249	0.022804	−0.000343	0.000263
0.100	0.000101	−0.000042	−0.000014	−0.026447	0.030989	−0.000473	0.000327

to the full BTE solutions when the umklapp scattering is dominant, it is still as much as 5% smaller than the full BTE solutions for Si and Ge [114]. The detailed values of our calculations are off from the experimental results, but the tendency of the thermal conductivity matches well with experiment.

Thermal conductivity calculated with the extended Hubbard functional is slightly larger than those of LDA and PBEsol over all temperature ranges considered (left column of Fig. 4). The thermal conductivity is determined basically by the phonon group velocity and lifetime. Our calculation shows that this behavior in the thermal conductivity mostly comes from the difference in the phonon lifetime. In the entire frequency range, we observe that the extended Hubbard functional produces a larger phonon lifetime than LDA or PBEsol (right column of Fig. 4). Our mode Grüneisen parameters calculated with the extended Hubbard functional are smaller in magnitude than those of LDA or PBEsol, and this result indicates the weaker phonon-phonon scattering and thus longer lifetimes for phonons depicted in the extended Hubbard functional. As discussed above, the weaker anharmonicity in the extended Hubbard functional than in LDA or GGA is evidence that the localization and delocalization of electrons are properly described by the extended Hubbard functional. The phonon group velocity also contributes to the thermal conductivity since the phonon bands calculated with the extended Hubbard functional have steeper dispersion in the acoustic branches than those of LDA or PBEsol.

V. CONCLUSION

We studied the lattice dynamics of group IV elements using a fully *ab initio* extended Hubbard functional. Calculated electronic band structures showed that the intersite Hubbard V term is essential for describing covalent-bonding orbital hybridization. Equilibrium lattice parameters, the bulk modulus, and energy gaps calculated with the extended Hubbard functional match experiment better than those calculated with other functionals.

The dynamical properties of group IV elements were also correctly described when the intersite V term in the extended Hubbard functional was considered. Our phonon frequencies calculated with the extended Hubbard functional show better agreement with experiment than those calculated with local, semilocal, or hybrid functionals. Mode Grüneisen parameters calculated with the extended Hubbard functional show a relatively large difference from those calculated with other functionals, especially in the acoustic branches of Si and Ge, where the values are negative. We expect that the extended Hubbard functional provides an accurate description of the thermal expansion of Si and Ge. We found that the phonon group velocity and lifetime calculated with the extended Hubbard functional are larger than those calculated with other functionals, and so is the lattice thermal conductivity. The extended Hubbard functional produces weaker anharmonicity than LDA or GGA, reflecting that it describes the localization and delocalization of electrons more properly than the mean-field-type functionals.

We note that the derivative of the U and V terms contributes little to the total forces and is not included in our force calculations. Rather, the Pulay forces from the derivatives of the occupation number were found to be crucial. For full consistency, the derivative of U and V with respect to atomic displacements may be necessary, in particular, for systems more correlated than conventional semiconductors.

ACKNOWLEDGMENTS

Y.-W.S. thanks B. G. Jang and S. Liu for fruitful discussions. S.-H.J. was supported by the National Research Foundation of Korea (NRF; Grant No. 2018R1A5A6075964) funded by the Korean government (MSIT). Y.-W.S. was supported by the NRF of Korea (Grant No. 2017R1A5A1014862,

TABLE VIII. The same as Table VI, but for total and Hubbard forces for Ge-Ge displacement.

		LOAO				NAO	
		F^N		F_{tot}		F^N	
R_K	$F^U + F^V$	+	−	+	−	+	−
0.025	0.000012	−0.000020	0.000019	−0.006064	0.006289	−0.000123	0.000115
0.050	0.000048	−0.000042	0.000035	−0.011910	0.012800	−0.000255	0.000218
0.075	0.000065	−0.000067	0.000048	−0.017520	0.019537	−0.000393	0.000309
0.100	0.000090	−0.000092	0.000057	−0.022885	0.026501	−0.000534	0.000387

SRC program: vdWMRC center) and KIAS individual Grant No. (CG031509). Supercomputing resources, including technical support, were provided by the Supercomputing Center, Korea Institute of Science and Technology Information (Contract No. KSC-2020-CRE-0173), and the Center for Advanced Computation of the Korea Institute for Advanced Study.

APPENDIX A: COMPARISON OF PULAY FORCES AND THE DERIVATIVE OF U AND V

We calculated the Hubbard force contribution from simplified $\mathbf{F}^U$ and $\mathbf{F}^V$ in Eqs. (12) and (13) for C, Si, and Ge. Tables VI, VII, and VIII show calculated $F^U = |\mathbf{F}^U|$, $F^V = |\mathbf{F}^V|$, and $F^N = |\mathbf{F}^N|$ using NAOs and LOAOs. The cutoff radius for evaluating the intersite Hubbard term V is set to include only the nearest-neighbor atoms in the ground configuration. F^U and F^V are calculated using the finite-difference method with a small displacement of $R_K = |\mathbf{R}_K|$ along the [111] direction. $F^U + F^V$ are similar in magnitude with F^N calculated with LOAOs, and both are much smaller than the total forces $F_{\text{tot}} = |dE_{\text{tot}}/d\mathbf{R}_K|$.

Without explicit formulas for the derivatives of U and V, it is hard to determine whether they can be neglected or not. The Hubbard correction terms are expressed in terms of the response function, which represents the change in the occupation number with respect to the potential shift [46]. As such, the force from the derivative of U and V may be non-negligible when the charge transfer or rebalancing between atomic orbitals becomes sensitive to atomic displacement. We expect such cases if flat degenerate bands are present near the Fermi level, as commonly observed in transition-metal oxides. As a quick test, we calculated the force for GaAs, NaCl, NiO, and FeO with a small atomic displacement of 0.1 bohr. We found that the derivative of U and V is negligible compared to the total force for GaAs and NaCl but relatively significant for NiO and FeO. The change in U is about 0.0006 eV for As (GaAs), whereas it is 0.0268 eV for Ni (NiO) for the same atomic displacement. A more thorough analysis is yet to be done.

APPENDIX B: ATOMIC ORBITAL BASIS IN THE CALCULATION OF HUBBARD FORCES

We discuss the choice of atomic-site projectors for force calculation of group IV semiconductors. The relaxed structures of Si with the NAO and LOAO have minor differences: the full relaxed lattice constants from the former and latter projectors are 5.439 and 5.434, respectively. When the overestimation of the occupation number is not crucial, the structure optimization with the NAO is expected to have marginal errors [30]. However, the phonon dispersions may be affected by the small change in forces.

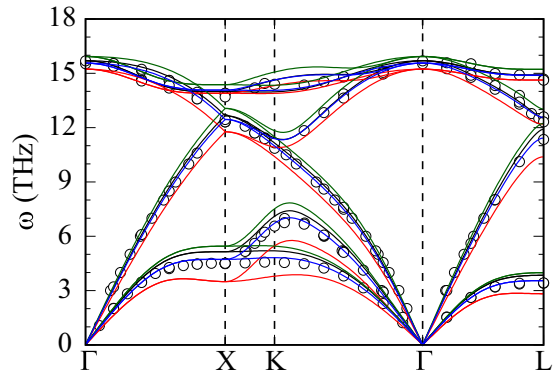

FIG. 5. The phonon bands of Si obtained at the experimental lattice constant using NAO (black), LOAO (blue), the derivative of only the inverse square root of the overlap matrix (red), and the derivative of only the atomic wave function (dark green). Open circles denote the measurement [91–93].

Figure 5 shows the phonon dispersion of Si at the experimental lattice constant. The Pulay forces using the NAO basis overestimate the phonon dispersion in the acoustic modes compared to measurement at ambient conditions. On the other hand, the Pulay forces [F^N in Eq. (9)] using the LOAO basis give agreeable phonon dispersion for entire modes. Moreover, the derivative of the inverse square root of the overlap matrix has a significant effect on the Pulay forces, as previously reported [43]. Without it, the overall phonon dispersion is overestimated compared to experiment. Both the derivative of the inverse square root of the overlap matrix and the derivative of the atomic wave functions should be included in the Pulay forces in the LOAO basis.

APPENDIX C: COMPARISON OF COMPUTATIONAL TIMES FOR EACH FUNCTIONAL

The computational time was compared for a single self-consistent loop for C, Si, and Ge, and we found that the extended Hubbard functional costs about 3, 3, and 1.4 times that of PBEsol, respectively, whereas HSE costs 142, 313, and 212 times that of PBEsol for the same calculation.

[1] P. Hohenberg and W. Kohn, Inhomogeneous electron gas, Phys. Rev. **136**, B864 (1964).
[2] W. Kohn and L. J. Sham, Self-consistent equations including exchange and correlation effects, Phys. Rev. **140**, A1133 (1965).
[3] R. O. Jones, Density functional theory: Its origins, rise to prominence, and future, Rev. Mod. Phys. **87**, 897 (2015).
[4] J. P. Perdew, K. Burke, and M. Ernzerhof, Generalized Gradient Approximation Made Simple, Phys. Rev. Lett. **77**, 3865 (1996).
[5] J. P. Perdew and A. Zunger, Self-interaction correction to density-functional approximations for many-electron systems, Phys. Rev. B **23**, 5048 (1981).
[6] P. Mori-Sánchez, A. J. Cohen, and W. Yang, Many-electron self-interaction error in approximate density functionals, J. Chem. Phys. **125**, 201102 (2006).
[7] J. Tao, J. P. Perdew, V. N. Staroverov, and G. E. Scuseria, Climbing the Density Functional Ladder: Nonempirical Meta–Generalized Gradient Approximation Designed for Molecules and Solids, Phys. Rev. Lett. **91**, 146401 (2003).

[8] J. P. Perdew, A. Ruzsinszky, G. I. Csonka, L. A. Constantin, and J. Sun, Workhorse Semilocal Density Functional for Condensed Matter Physics and Quantum Chemistry, Phys. Rev. Lett. **103**, 026403 (2009).

[9] J. Sun, B. Xiao, and A. Ruzsinszky, Communication: Effect of the orbital-overlap dependence in the meta generalized gradient approximation, J. Chem. Phys. **137**, 051101 (2012).

[10] Y. Zhao and D. G. Truhlar, A new local density functional for main-group thermochemistry, transition metal bonding, thermochemical kinetics, and noncovalent interactions, J. Chem. Phys. **125**, 194101 (2006).

[11] J. M. del Campo, J. L. Gázquez, S. Trickey, and A. Vela, A new meta-GGA exchange functional based on an improved constraint-based GGA, Chem. Phys. Lett. **543**, 179 (2012).

[12] J. Sun, A. Ruzsinszky, and J. P. Perdew, Strongly Constrained and Appropriately Normed Semilocal Density Functional, Phys. Rev. Lett. **115**, 036402 (2015).

[13] J. Heyd, G. E. Scuseria, and M. Ernzerhof, Hybrid functionals based on a screened Coulomb potential, J. Chem. Phys. **118**, 8207 (2003).

[14] A. V. Krukau, O. A. Vydrov, A. F. Izmaylov, and G. E. Scuseria, Influence of the exchange screening parameter on the performance of screened hybrid functionals, J. Chem. Phys. **125**, 224106 (2006).

[15] B. G. Janesko, T. M. Henderson, and G. E. Scuseria, Screened hybrid density functionals for solid-state chemistry and physics, Phys. Chem. Chem. Phys. **11**, 443 (2009).

[16] M. Jain, J. R. Chelikowsky, and S. G. Louie, Reliability of Hybrid Functionals in Predicting Band Gaps, Phys. Rev. Lett. **107**, 216806 (2011).

[17] L. Hedin, New method for calculating the one-particle Green's function with application to the electron-gas problem, Phys. Rev. **139**, A796 (1965).

[18] M. S. Hybertsen and S. G. Louie, Electron correlation in semiconductors and insulators: Band gaps and quasiparticle energies, Phys. Rev. B **34**, 5390 (1986).

[19] M. Shishkin, M. Marsman, and G. Kresse, Accurate Quasiparticle Spectra from Self-Consistent *GW* Calculations with Vertex Corrections, Phys. Rev. Lett. **99**, 246403 (2007).

[20] G. Kotliar, S. Y. Savrasov, K. Haule, V. S. Oudovenko, O. Parcollet, and C. A. Marianetti, Electronic structure calculations with dynamical mean-field theory, Rev. Mod. Phys. **78**, 865 (2006).

[21] V. I. Anisimov, J. Zaanen, and O. K. Andersen, Band theory and Mott insulators: Hubbard U instead of Stoner I, Phys. Rev. B **44**, 943 (1991).

[22] V. I. Anisimov, F. Aryasetiawan, and A. I. Lichtenstein, First-principles calculations of the electronic structure and spectra of strongly correlated systems: The LDA + U method, J. Phys.: Condens. Matter **9**, 767 (1997).

[23] S. L. Dudarev, G. A. Botton, S. Y. Savrasov, C. J. Humphreys, and A. P. Sutton, Electron-energy-loss spectra and the structural stability of nickel oxide: An LSDA+U study, Phys. Rev. B **57**, 1505 (1998).

[24] B. Himmetoglu, A. Floris, S. de Gironcoli, and M. Cococcioni, Hubbard-corrected DFT energy functionals: The LDA + U description of correlated systems, Int. J. Quantum Chem. **114**, 14 (2014).

[25] V. L. Campo, Jr., and M. Cococcioni, Extended DFT + U + V method with on-site and inter-site electronic interactions, J. Phys.: Condens. Matter **22**, 055602 (2010).

[26] S.-H. Lee and Y.-W. Son, First-principles approach with a pseudohybrid density functional for extended Hubbard interactions, Phys. Rev. Res. **2**, 043410 (2020).

[27] N. Tancogne-Dejean and A. Rubio, Parameter-free hybridlike functional based on an extended Hubbard model: DFT + U + V, Phys. Rev. B **102**, 155117 (2020).

[28] I. Timrov, N. Marzari, and M. Cococcioni, Self-consistent Hubbard parameters from density-functional perturbation theory in the ultrasoft and projector-augmented wave formulations, Phys. Rev. B **103**, 045141 (2021).

[29] H. J. Kulik and N. Marzari, Transition-metal dioxides: A case for the intersite term in Hubbard-model functionals, J. Chem. Phys. **134**, 094103 (2011).

[30] M. Cococcioni and N. Marzari, Energetics and cathode voltages of LiMPO$_4$ olivines (M = Fe, Mn) from extended Hubbard functionals, Phys. Rev. Mater. **3**, 033801 (2019).

[31] C. Ricca, I. Timrov, M. Cococcioni, N. Marzari, and U. Aschauer, Self-consistent DFT + U + V study of oxygen vacancies in SrTiO$_3$, Phys. Rev. Res. **2**, 023313 (2020).

[32] I. Timrov, P. Agrawal, X. Zhang, S. Erat, R. Liu, A. Braun, M. Cococcioni, M. Calandra, N. Marzari, and D. Passerone, Electronic structure of pristine and Ni-substituted LaFeO$_3$ from near edge x-ray absorption fine structure experiments and first-principles simulations, Phys. Rev. Res. **2**, 033265 (2020).

[33] H. J. Kulik, M. Cococcioni, D. A. Scherlis, and N. Marzari, Density Functional Theory in Transition-Metal Chemistry: A Self-Consistent Hubbard U Approach, Phys. Rev. Lett. **97**, 103001 (2006).

[34] M. Cococcioni and S. de Gironcoli, Linear response approach to the calculation of the effective interaction parameters in the LDA + U method, Phys. Rev. B **71**, 035105 (2005).

[35] I. Timrov, N. Marzari, and M. Cococcioni, Hubbard parameters from density-functional perturbation theory, Phys. Rev. B **98**, 085127 (2018).

[36] T. Miyake and F. Aryasetiawan, Screened Coulomb interaction in the maximally localized Wannier basis, Phys. Rev. B **77**, 085122 (2008).

[37] T. Miyake, F. Aryasetiawan, and M. Imada, *Ab initio* procedure for constructing effective models of correlated materials with entangled band structure, Phys. Rev. B **80**, 155134 (2009).

[38] M. Aichhorn, L. Pourovskii, V. Vildosola, M. Ferrero, O. Parcollet, T. Miyake, A. Georges, and S. Biermann, Dynamical mean-field theory within an augmented plane-wave framework: Assessing electronic correlations in the iron pnictide LaFeAsO, Phys. Rev. B **80**, 085101 (2009).

[39] N. J. Mosey and E. A. Carter, *Ab initio* evaluation of Coulomb and exchange parameters for DFT + U calculations, Phys. Rev. B **76**, 155123 (2007).

[40] N. J. Mosey, P. Liao, and E. A. Carter, Rotationally invariant ab initio evaluation of Coulomb and exchange parameters for DFT + U calculations, J. Chem. Phys. **129**, 014103 (2008).

[41] L. A. Agapito, S. Curtarolo, and M. Buongiorno Nardelli, Reformulation of DFT + U as a Pseudohybrid Hubbard Density Functional for Accelerated Materials Discovery, Phys. Rev. X **5**, 011006 (2015).

[42] Y.-C. Wang, Z.-H. Chen, and H. Jiang, The local projection in the density functional theory plus U approach: A critical assessment, J. Chem. Phys. **144**, 144106 (2016).

[43] I. Timrov, F. Aquilante, L. Binci, M. Cococcioni, and N. Marzari, Pulay forces in density-functional theory with extended Hubbard functionals: From nonorthogonalized to orthogonalized manifolds, Phys. Rev. B **102**, 235159 (2020).

[44] P. Löwdin, On the non-orthogonality problem connected with the use of atomic wave functions in the theory of molecules and crystals, J. Chem. Phys. **18**, 365 (1950).

[45] I. Mayer, On Löwdin's method of symmetric orthogonalization, Int. J. Quantum Chem. **90**, 63 (2002).

[46] H. J. Kulik and N. Marzari, Accurate potential energy surfaces with a DFT+$U(R)$ approach, J. Chem. Phys. **135**, 194105 (2011).

[47] P. Giannozzi *et al.*, QUANTUM ESPRESSO: A modular and open-source software project for quantum simulations of materials, J. Phys.: Condens. Matter **21**, 395502 (2009).

[48] M. van Setten, M. Giantomassi, E. Bousquet, M. Verstraete, D. Hamann, X. Gonze, and G.-M. Rignanese, The PseudoDojo: Training and grading a 85 element optimized norm-conserving pseudopotential table, Comput. Phys. Commun. **226**, 39 (2018).

[49] P. Vinet, J. H. Rose, J. Ferrante, and J. R. Smith, Universal features of the equation of state of solids, J. Phys.: Condens. Matter **1**, 1941 (1989).

[50] N. Marzari, A. A. Mostofi, J. R. Yates, I. Souza, and D. Vanderbilt, Maximally localized Wannier functions: Theory and applications, Rev. Mod. Phys. **84**, 1419 (2012).

[51] G. Pizzi *et al.*, Wannier90 as a community code: New features and applications, J. Phys.: Condens. Matter **32**, 165902 (2020).

[52] K. Esfarjani and H. T. Stokes, Method to extract anharmonic force constants from first principles calculations, Phys. Rev. B **77**, 144112 (2008).

[53] L. Lindsay, D. A. Broido, and T. L. Reinecke, Thermal Conductivity and Large Isotope Effect in GaN from First Principles, Phys. Rev. Lett. **109**, 095901 (2012).

[54] D. A. Broido, M. Malorny, G. Birner, N. Mingo, and D. A. Stewart, Intrinsic lattice thermal conductivity of semiconductors from first principles, Appl. Phys. Lett. **91**, 231922 (2007).

[55] A. Ward, D. A. Broido, D. A. Stewart, and G. Deinzer, *Ab initio* theory of the lattice thermal conductivity in diamond, Phys. Rev. B **80**, 125203 (2009).

[56] L. Lindsay, D. A. Broido, and N. Mingo, Diameter dependence of carbon nanotube thermal conductivity and extension to the graphene limit, Phys. Rev. B **82**, 161402(R) (2010).

[57] L. Lindsay, D. A. Broido, and N. Mingo, Flexural phonons and thermal transport in multilayer graphene and graphite, Phys. Rev. B **83**, 235428 (2011).

[58] L. Lindsay and D. A. Broido, Theory of thermal transport in multilayer hexagonal boron nitride and nanotubes, Phys. Rev. B **85**, 035436 (2012).

[59] W. Li, N. Mingo, L. Lindsay, D. A. Broido, D. A. Stewart, and N. A. Katcho, Thermal conductivity of diamond nanowires from first principles, Phys. Rev. B **85**, 195436 (2012).

[60] D. A. Broido, L. Lindsay, and A. Ward, Thermal conductivity of diamond under extreme pressure: A first-principles study, Phys. Rev. B **86**, 115203 (2012).

[61] S. Poncé, E. R. Margine, and F. Giustino, Towards predictive many-body calculations of phonon-limited carrier mobilities in semiconductors, Phys. Rev. B **97**, 121201(R) (2018).

[62] S. Poncé, W. Li, S. Reichardt, and F. Giustino, First-principles calculations of charge carrier mobility and conductivity in bulk semiconductors and two-dimensional materials, Rep. Prog. Phys. **83**, 036501 (2020).

[63] T. Tadano, Y. Gohda, and S. Tsuneyuki, Anharmonic force constants extracted from first-principles molecular dynamics: Applications to heat transfer simulations, J. Phys.: Condens. Matter **26**, 225402 (2014).

[64] A. Ward and D. A. Broido, Intrinsic phonon relaxation times from first-principles studies of the thermal conductivities of Si and Ge, Phys. Rev. B **81**, 085205 (2010).

[65] L. Chaput, Direct Solution to the Linearized Phonon Boltzmann Equation, Phys. Rev. Lett. **110**, 265506 (2013).

[66] A. Togo, L. Chaput, and I. Tanaka, Distributions of phonon lifetimes in Brillouin zones, Phys. Rev. B **91**, 094306 (2015).

[67] B. J. Skinner, The thermal expansions of thoria, periclase and diamond, Am. Min. **42**, 39 (1957).

[68] P. Becker, P. Scyfried, and H. Siegert, The lattice parameter of highly pure silicon single crystals, Z. Phys. B **48**, 17 (1982).

[69] M. Y. Hu, H. Sinn, A. Alatas, W. Sturhahn, E. E. Alp, H. C. Wille, Y. V. Shvyd'ko, J. P. Sutter, J. Bandaru, E. E. Haller, V. I. Ozhogin, S. Rodriguez, R. Colella, E. Kartheuser, and M. A. Villeret, Effect of isotopic composition on the lattice parameter of germanium measured by x-ray backscattering, Phys. Rev. B **67**, 113306 (2003).

[70] M. H. Grimsditch and A. K. Ramdas, Brillouin scattering in diamond, Phys. Rev. B **11**, 3139 (1975).

[71] M. Senoo, H. Mii, I. Fujishiro, and T. Fujikawa, Precise measurements of lattice compression of Al, Si and Al-Si alloys by high pressure x-ray diffractometry, Jpn. J. Appl. Phys. **15**, 871 (1976).

[72] A. K. Singh and G. C. Kennedy, Compressions of Si, MgO, and ZrSiO 4 to 8 GPa as measured with a WC-anvil x-ray apparatus and epoxy pressure medium, J. Appl. Phys. **48**, 3362 (1977).

[73] L. J. Bruner and R. W. Keyes, Electronic Effect in the Elastic Constants of Germanium, Phys. Rev. Lett. **7**, 55 (1961).

[74] H. J. McSkimin and P. Andreatch, Elastic moduli of germanium versus hydrostatic pressure at 25.0 °C and −195.8 °C, J. Appl. Phys. **34**, 651 (1963).

[75] K. Hummer, J. Harl, and G. Kresse, Heyd-Scuseria-Ernzerhof hybrid functional for calculating the lattice dynamics of semiconductors, Phys. Rev. B **80**, 115205 (2009).

[76] J. Heyd and G. E. Scuseria, Efficient hybrid density functional calculations in solids: Assessment of the Heyd–Scuseria–Ernzerhof screened Coulomb hybrid functional, J. Chem. Phys. **121**, 1187 (2004).

[77] J. Heyd, J. E. Peralta, G. E. Scuseria, and R. L. Martin, Energy band gaps and lattice parameters evaluated with the Heyd-Scuseria-Ernzerhof screened hybrid functional, J. Chem. Phys. **123**, 174101 (2005).

[78] F. Tran, R. Laskowski, P. Blaha, and K. Schwarz, Performance on molecules, surfaces, and solids of the Wu-Cohen GGA exchange-correlation energy functional, Phys. Rev. B **75**, 115131 (2007).

[79] P. Haas, F. Tran, and P. Blaha, Calculation of the lattice constant of solids with semilocal functionals, Phys. Rev. B **79**, 085104 (2009).

[80] C. D. Clark, P. J. Dean, and P. V. Harris, Intrinsic edge absorption in diamond, Proc. R. Soc. London, Ser. A **277**, 312 (1964).

[81] R. A. Roberts and W. C. Walker, Optical study of the electronic structure of diamond, Phys. Rev. **161**, 730 (1967).
[82] T. P. McLean, The absorption edge spectrum of semiconductors, Prog. Semicond. **5**, 55 (1960).
[83] A. Daunois and D. E. Aspnes, Electroreflectance and ellipsometry of silicon from 3 to 6 eV, Phys. Rev. B **18**, 1824 (1978).
[84] G. G. Macfarlane, T. P. McLean, J. E. Quarrington, and V. Roberts, Fine structure in the absorption-edge spectrum of Ge, Phys. Rev. **108**, 1377 (1957).
[85] J. Camassel and D. Auvergne, Temperature dependence of the fundamental edge of germanium and zinc-blende-type semiconductors, Phys. Rev. B **12**, 3258 (1975).
[86] M. Rohlfing, P. Krüger, and J. Pollmann, Quasiparticle band-structure calculations for C, Si, Ge, GaAs, and SiC using Gaussian-orbital basis sets, Phys. Rev. B **48**, 17791 (1993).
[87] Y.-S. Kim, M. Marsman, G. Kresse, F. Tran, and P. Blaha, Towards efficient band structure and effective mass calculations for III-V direct band-gap semiconductors, Phys. Rev. B **82**, 205212 (2010).
[88] J. L. Warren, J. L. Yarnell, G. Dolling, and R. A. Cowley, Lattice dynamics of diamond, Phys. Rev. **158**, 805 (1967).
[89] J. Kulda, B. Dorner, B. Roessli, H. Sterner, R. Bauer, T. May, K. Karch, P. Pavone, and D. Strauch, A neutron-scattering study of the overbending of the [100] LO phonon mode in diamond, Solid State Commun. **99**, 799 (1996).
[90] J. Kulda, H. Kainzmaier, D. Strauch, B. Dorner, M. Lorenzen, and M. Krisch, Overbending of the longitudinal optical phonon branch in diamond as evidenced by inelastic neutron and x-ray scattering, Phys. Rev. B **66**, 241202(R) (2002).
[91] G. Dolling, *Inelastic Scattering of Neutrons in Solids and Liquids* (International Atomic Energy Agency, Vienna, 1963).
[92] G. Nilsson and G. Nelin, Study of the homology between silicon and germanium by thermal-neutron spectrometry, Phys. Rev. B **6**, 3777 (1972).
[93] J. Kulda, D. Strauch, P. Pavone, and Y. Ishii, Inelastic-neutron-scattering study of phonon eigenvectors and frequencies in Si, Phys. Rev. B **50**, 13347 (1994).
[94] G. Nilsson and G. Nelin, Phonon dispersion relations in Ge at 80 °K, Phys. Rev. B **3**, 364 (1971).
[95] K. Nakano, T. Morresi, M. Casula, R. Maezono, and S. Sorella, Atomic forces by quantum Monte Carlo: Application to phonon dispersion calculations, Phys. Rev. B **103**, L121110 (2021).
[96] C. H. Xu, C. Z. Wang, C. T. Chan, and K. M. Ho, Theory of the thermal expansion of Si and diamond, Phys. Rev. B **43**, 5024 (1991).
[97] G.-M. Rignanese, J.-P. Michenaud, and X. Gonze, *Ab initio* study of the volume dependence of dynamical and thermodynamical properties of silicon, Phys. Rev. B **53**, 4488 (1996).
[98] M. H. Grimsditch, E. Anastassakis, and M. Cardona, Effect of uniaxial stress on the zone-center optical phonon of diamond, Phys. Rev. B **18**, 901 (1978).
[99] S. S. Mitra, O. Brafman, W. B. Daniels, and R. K. Crawford, Pressure-induced phonon frequency shifts measured by Raman scattering, Phys. Rev. **186**, 942 (1969).
[100] E. Whalley, A. Lavergne, and P. T. T. Wong, Hydrostatic optical cell with glass windows for 25 kilobar, Rev. Sci. Instrum. **47**, 845 (1976).
[101] B. A. Weinstein and G. J. Piermarini, Raman scattering and phonon dispersion in Si and GaP at very high pressure, Phys. Rev. B **12**, 1172 (1975).
[102] W. Richter, J. Renucci, and M. Cardona, Pressure dependence of the zone edge TA phonons in silicon, Solid State Commun. **16**, 131 (1975).
[103] D. Olego and M. Cardona, Pressure dependence of Raman phonons of Ge and 3*C*-SiC, Phys. Rev. B **25**, 1151 (1982).
[104] R. T. Payne, Phonon energies in germanium from phonon-assisted tunneling, Phys. Rev. **139**, A570 (1965).
[105] P. Mori-Sánchez, A. J. Cohen, and W. Yang, Localization and Delocalization Errors in Density Functional Theory and Implications for Band-Gap Prediction, Phys. Rev. Lett. **100**, 146401 (2008).
[106] J. R. Olson, R. O. Pohl, J. W. Vandersande, A. Zoltan, T. R. Anthony, and W. F. Banholzer, Thermal conductivity of diamond between 170 and 1200 K and the isotope effect, Phys. Rev. B **47**, 14850 (1993).
[107] L. Wei, P. K. Kuo, R. L. Thomas, T. R. Anthony, and W. F. Banholzer, Thermal Conductivity of Isotopically Modified Single Crystal Diamond, Phys. Rev. Lett. **70**, 3764 (1993).
[108] A. V. Inyushkin, A. N. Taldenkov, J. W. Ager, E. E. Haller, H. Riemann, N. V. Abrosimov, H.-J. Pohl, and P. Becker, Ultrahigh thermal conductivity of isotopically enriched silicon, J. Appl. Phys. **123**, 095112 (2018).
[109] V. I. Ozhogin, A. V. Inyushkin, A. N. Taldenkov, A. V. Tikhomirov, G. Popov, E. Haller, and K. Itoh, Isotope effect in the thermal conductivity of germanium single crystals, JETP Lett. **63**, 490 (1996).
[110] M. Asen-Palmer, K. Bartkowski, E. Gmelin, M. Cardona, A. P. Zhernov, A. V. Inyushkin, A. Taldenkov, V. I. Ozhogin, K. M. Itoh, and E. E. Haller, Thermal conductivity of germanium crystals with different isotopic compositions, Phys. Rev. B **56**, 9431 (1997).
[111] A. Ward, First principles theory of the lattice thermal conductivity of semiconductors, Ph.D. thesis, Boston College, 2009.
[112] L. Lindsay, D. A. Broido, and T. L. Reinecke, *Ab initio* thermal transport in compound semiconductors, Phys. Rev. B **87**, 165201 (2013).
[113] A. Jain and A. J. McGaughey, Effect of exchange–correlation on first-principles-driven lattice thermal conductivity predictions of crystalline silicon, Comput. Mater. Sci. **110**, 115 (2015).
[114] J. Carrete, B. Vermeersch, A. Katre, A. van Roekeghem, T. Wang, G. K. Madsen, and N. Mingo, almaBTE: A solver of the space–time dependent Boltzmann transport equation for phonons in structured materials, Comput. Phys. Commun. **220**, 351 (2017).